Title

Application of flow sensitive gradients for improved measures of metabolism using hyperpolarized (13) c MRI.

Journal

Magnetic Resonance in Medicine, 75(3)

Authors

Gordon, Jeremy
Niles, David
Adamson, Erin
et al.

Publication Date

2016-03-01

DOI

10.1002/mrm.25584

Peer reviewed

HHS Public Access

Author manuscript

Magn Reson Med. Author manuscript; available in PMC 2016 March 01.

Published in final edited form as:

Magn Reson Med. 2016 March ; 75(3): 1242–1248. doi:10.1002/mrm.25584.

Application of Flow Sensitive Gradients for Improved Measures of Metabolism Using Hyperpolarized ^{13}C MRI

Jeremy W. Gordon[1], **David J. Niles**[1], **Erin B. Adamson**[1], **Kevin M. Johnson**[1], and **Sean B. Fain**[1,2,3]

[1]Medical Physics, University of Wisconsin-Madison, Madison, WI, United States

[2]Radiology, University of Wisconsin-Madison, Madison, WI, United States

[3]Biomedical Engineering, University of Wisconsin-Madison, Madison, WI, United States

Abstract

Purpose—To develop the use of bipolar gradients to suppress partial-volume and flow-related artifacts from macro-vascular, hyperpolarized spins.

Methods—Digital simulations were performed over a range of spatial resolutions and gradient strengths to determine the optimal bipolar gradient strength and duration to suppress flowing spins while minimizing signal loss from static tissue. In-vivo experiments were performed to determine the efficacy of this technique to suppress vascular signal in the study of hyperpolarized [1-^{13}C]pyruvate renal metabolism.

Results—Digital simulations showed that in the absence of bipolar gradients, partial-volume artifacts from the vasculature were still present, causing underestimation of the apparent reaction rate of pyruvate to lactate (k_P). The addition of a bipolar gradient with b = 32 s/mm^2 sufficiently suppressed the vascular signal without a substantial decrease in signal from static tissue. In-vivo results corroborate digital simulations, with similar peak lactate SNR but substantially different k_P in the presence of bipolar gradients.

Conclusion—The proposed approach suppresses signal from flowing spins while minimizing signal loss from static tissue, removing contaminating signal from the vasculature and increasing kinetic modeling accuracy without substantially sacrificing SNR or temporal resolution.

Keywords

Metabolism; Pyruvate; DNP; Diffusion; Vascular Suppression; Hyperpolarization

INTRODUCTION

Advances in hyperpolarization (1) have enabled rapid, non-invasive imaging of ^{13}C metabolism, most commonly the flux of pyruvate through lactate dehydrogenase and citric acid pathways. Hyperpolarized ^{13}C techniques hold potential as biomarkers of metabolic

Corresponding Author and Reprint Info: Sean Fain, University of Wisconsin – Madison, 1113 Wisconsin Institutes Medical Research, 1111 Highland Ave., Department of MR/CT Research, Madison, WI 53705, Phone: (608)-263-0090, sfain@wisc.edu.

abnormalities in cancer (2–7), liver (8), renal (9), and cardiac (10) disease. Nevertheless, the translation of ^{13}C to clinical application faces several substantial challenges. A major drawback of hyperpolarized ^{13}C imaging is the tradeoff between spatial and temporal resolution made necessary by the rapid decay of hyperpolarized signal due to metabolism, T_1 relaxation and RF saturation. As a result, only coarse spatial resolution can be obtained for dynamic time-resolved imaging, leading to significant partial-volume mixing between tissue and blood compartments. These contributions can lead to errors in the quantification of metabolic rates within the tissues of interest (11).

Blood pool suppression would be valuable for ^{13}C quantification; unfortunately, the adaptation of existing suppression techniques developed for conventional imaging (12) is non-trivial due to the transient nature of the hyperpolarized signal. Several novel techniques for suppressing vascular signals in hyperpolarized applications have been proposed. For example, outer volume pre-saturation of metabolites has been shown to mitigate bias due to circulation of metabolic products (13), though this method does not suppress the strong vascular component from the hyperpolarized substrate itself (e.g. pyruvate). Paramagnetic agents such as gadolinium have also been used to suppress signal from the vasculature (14). However, this technique reduces the ^{13}C T_1 due to interaction with the contrast agent, accelerating the rate of decay and shortening the available imaging time. Alternatively, double spin-echo (15) and stimulated-echo techniques (STEAM) have been applied to remove signal from flowing spins by motion-dependent phase accrual (16,17). These techniques can provide excellent suppression of moving spins, but utilize multiple 90° or 180° excitations that are temporally inefficient and are sensitive to timing, motion and B_1 inhomogeneity.

Ideal vascular suppression techniques would suppress macro-vascular signal and allow for efficient and rapid dynamic imaging. In ^{1}H MRI, bipolar gradients have been used to suppress macro-vascular signal to improve measures of capillary perfusion (18,19) and increase conspicuity of vessel walls (20). Unlike spin-echo sensitization, this approach allows low flip angle excitation and may be well suited for hyperpolarized experiments. In conjunction with the relatively coarse resolution in hyperpolarized ^{13}C experiments, bipolar gradients should improve quantitative measures of metabolism by suppressing vascular spins. However, these gradients will lead to some measure of signal loss due to extended echo times and diffusion sensitization, requiring a balance between maximizing vascular suppression and mitigating diffusion related signal loss.

In this work, we investigate the use of bipolar gradients to suppress partial-volume and flow-related artifacts from macro-vascular hyperpolarized [1-^{13}C]pyruvate, with focus on the study of renal metabolism. Digital simulations were used to assess the degree of partial-volume mixing on measures of renal metabolism and to explore the tradeoff between vascular suppression via flow dephasing and diffusion weighting. In-vivo imaging experiments of renal metabolism were performed to validate the technique.

THEORY

Signal loss from bipolar gradients is a combination of flow-dependent phase dispersion from bulk flow within vessels and diffusion from Brownian motion. The bipolar gradients cause phase accumulation in flowing spins, with a velocity-induced phase accrual Φ_v equal to:

$$\Phi_v = \gamma m_1 v(x) \quad \text{Eq. 1}$$

$$m_1 = \int_0^{2T} G(t) t \, dt \quad \text{Eq. 2}$$

where γ is the gyromagnetic ratio, m_1 is the first gradient moment, $v(x)$ is the voxel dependent velocity at position x, $G(t)$ is the time-dependent gradient amplitude and T is the duration of a single lobe of the bipolar pulse, assuming no delay between the lobes. For vessels of size comparable to a voxel, the intravoxel velocity profile is not spatially uniform. As is well understood from phase contrast (PC) velocimetry, the intra-voxel distribution of velocities can lead to substantial signal loss with high first moments or large voxels (21–23). The net signal loss can be approximated by the spread in intravoxel velocities:

$$S(\Delta v) = S_0 \int_0^{v_{\max}} exp\left(-i\gamma m_1 v\right) dv \quad \text{Eq. 3a}$$

$$S(\Delta v) = S_0 \left|\mathrm{sinc}(\gamma m_1 \Delta v/2)\right| \quad \text{Eq. 3b}$$

where S_0 is the signal in the absence of bipolar gradients and Δv is the intra-voxel velocity profile for a given voxel. This signal loss is substantially higher in areas of blood acceleration, turbulence, or complex flow patterns.

In addition to bulk flow effects, bipolar gradient pulses sensitize spins to molecular diffusion depending on its b-value (24,25). The resulting signal is attenuated due to Brownian motion, with the fractional signal S remaining in each voxel calculated as (26)

$$S(d) = S_0 \, exp(-bd(x)) \quad \text{Eq. 4}$$

$$b = \gamma^2 G_{diff}^2 \left(\frac{2\delta^3}{3} + \delta^2\xi + \frac{\xi^3}{30} - \frac{\xi^2\delta}{6}\right) \quad \text{Eq. 5}$$

where $d(x)$ is the voxel-dependent diffusion coefficient within a given voxel at position x and b is calculated for trapezoidal gradients. In this nomenclature, G_{diff} is the peak gradient amplitude and ξ is the ramp duration, with $T = \delta + \xi$. Therefore, increasing vascular suppression will lead to a concomitant signal decrease from slow or non-flowing spins. Due to the relationship of the first gradient moment and b to the bipolar pulse parameters γ, G, δ and ξ, there is a necessary tradeoff between increased vascular suppression and signal loss from static spins. Furthermore, the first moment scales linearly with gradient strength while the b-value scales quadratically, such that diffusion weighting increases faster than vascular

suppression. Therefore, an empirical balance must be sought between phase dispersion and diffusion weighting to maximize suppression of flowing spins in the large vessels while mitigating diffusion weighting of spins in the metabolically active tissues.

METHODS

All experiments used a spiral gradient-echo sequence with bipolar gradients inserted on all three axes developed for use on a 4.7 T small animal scanner (Agilent, Palo Alto, CA, USA) with high performance gradients (maximum amplitude = 400 mT/m, maximum slew-rate = 2580 T/m/s). For both simulations and in-vivo studies, ^{13}C data were acquired with a constant density spiral trajectory (27). Five unique echoes were acquired per timeframe spaced a ΔTE of 1.19 ms apart to optimize the phase differences and maximize the effective number of signal averages (28).

To simulate the expected effect of partial-voluming on kinetic modeling with hyperpolarized metabolites, a two-site exchange model (6) was implemented in Matlab (R2009b, MathWorks, Natick, MA, USA). Masks of the kidney body and abdominal aorta were obtained from a high-resolution (0.125 × 0.125 mm^2) axial ^1H image of the kidneys. Spiral data acquisitions of [1-^{13}C]pyruvate and metabolites were simulated with and without applied bipolar gradients of b-value = 32 s/mm^2 (G = 360 mT/m, δ = 2.96 ms, ξ = 0.14 ms), assuming a ^{13}C T_2* of 20 ms and peak blood velocity of 30 cm/s (29). Zero-mean Gaussian noise was added to simulated k-space data to achieve realistic SNR. Signal loss due to Brownian motion was assumed using a diffusion coefficient of 1.12×10^{-3} mm^2/s (30). Data were simulated over a range of in-plane resolutions (4×4 mm^2, 2×2 mm^2, 1×1 mm^2) to determine the degree of sensitivity of kinetic modeling on partial-volume artifacts arising from the abdominal aorta.

In-vivo hyperpolarized [1-^{13}C]pyruvate MRI experiments of murine renal metabolism were performed to assess the in-vivo efficacy of bipolar vascular suppression. Prior to ^{13}C experiments, an empirical b-value was confirmed from ^1H imaging using a gradient echo sequence with bipolar gradients on all three axes. Scan parameters were TR/TE = 30/6.9 ms, G_{diff} = 170 mT/m, δ = 1.93 ms and ξ = 0.07 ms. This corresponds to a b-value of 32 s/mm^2 and a VENC of 0.9 cm/s.

30 μL aliquots of [1-^{13}C]pyruvic acid (Sigma-Aldrich, St. Louis, MO) and 15 mM trityl radical (Ox063, GE Healthcare) were polarized for one hour in a Hypersense polarizer (Oxford Instruments, Tubney Woods, Abingdon, Oxfordshire, UK). Samples were dissoluted with 4 mL solvent comprised of 100 mM NaOH, 80 mM Tris buffer and 250 mg/L EDTA. [1-^{13}C]pyruvate was drawn off and 10 μL/g was rapidly injected into healthy ICR mice via tail-vein cannulation. Animals were anesthetized with 1.5% isofluorane and maintained at 36.5 ± 0.5 °C for the duration of the experiment. All animal experiments were conducted in compliance with the Institutional Animal Care and Use Committee. Liquid-state polarization was measured at the start of injection with a benchtop polarimeter (Oxford Instruments, Tubney Woods, Abingdon, Oxfordshire, UK).

Hyperpolarized ^{13}C images of four chemical species ([1-^{13}C]pyruvate, [1-^{13}C]pyruvate hydrate, [1-^{13}C]alanine, and [1-^{13}C]lactate) were acquired using a constant density spiral readout with one echo per excitation, a readout duration of 41 ms. The spiral readout was generated for a nominal resolution of 2×2×10 mm^3, but due to T_2* decay (on the order of 20 ms) the actual in-plane resolution is twofold coarser, resulting in a voxel size of 4×4×10 mm^3. A 10°, 300 μs sinc RF pulse was used to excite ^{13}C species while minimizing chemical-shift artifacts in the slice-select direction. Experiments were performed with (TR/TE_1 = 55/7.0 ms) and without (TR/TE_1 = 55/0.55 ms) diffusion gradients (G_{diff} = 360 mT/m, δ = 2.96 ms, ζ = 0.14 ms) on all three axes, corresponding to a b-value of 32 s/mm^2 and a VENC of 0.7 cm/s. Data acquisition started 20 s prior to the start of injection, and timeframes were acquired every 4 s. Dynamic ^{13}C datasets were corrected for signal loss due to RF excitation by multiplying by $1/cos^{(n-1)}\theta$ (31) and reconstructed with a least-squares estimation technique (32,33). To account for gradient infidelity and timing delays, the k-space trajectory was measured on the ^1H channel using a thin-slice excitation method (34). A B_0 field-map estimated from ^1H data using a gradient-echo sequence ($TR/TE_1/\Delta TE$ = 15 ms/4.3 ms/0.5 ms, 8 echoes, 0.25×0.25×2.0 mm^3 resolution) was acquired prior to ^{13}C imaging to correct the spiral data for field inhomogeneities. Reconstructed metabolite maps were masked based on the high-resolution ^1H data acquired prior to ^{13}C imaging. The mean pyruvate and lactate signal from both kidneys was calculated at each timeframe and fit to the two-site exchange model discussed above.

RESULTS

The tradeoff between vascular suppression and sensitization to diffusion described by the equations above is depicted graphically in Fig. 1. To minimize signal loss due to T_2^* relaxation, flow suppression calculations assumed a fixed peak gradient amplitude of 360 mT/m. This results in a large parameter space where vascular signal is suppressed over a range of velocities with minimal effect on static spins (Fig. 1B). A b-value of 32 s/mm^2, corresponding to G_{diff} = 360 mT/m and T = 3.1 ms, was chosen to maximize suppression in both fast spins in the descending aorta as well as slower flowing spins. Note that for the expected velocity in the descending aorta, intra-voxel phase dispersion greater than 6π in the direction of motion is sufficient to suppress at least 80% of the signal from flowing spins (Fig. 2).

Digital simulations of renal metabolism showed that even with a relatively high in-plane resolution of 2×2 mm^2, partial-volume artifacts from the vasculature were still present without using bipolar gradients (Fig. 3), leading to an underestimation of the apparent reaction rate of pyruvate to lactate (k_P; Supporting Table S1). Improving spatial resolution mitigated partial-volume effects (Fig. 3 A and B, top row, far right column) without bipolar gradients as expected, but the poor SNR resulting from the small voxel size reduced image quality for the highest resolution studied (1×1 mm^2). The addition of a bipolar gradient with b = 32 s/mm^2 is shown to suppress the vascular signal sufficiently to remove the remaining partial-volume effects as predicted analytically (Fig. 3 A and B, bottom row) without a substantial SNR penalty. Kinetic modeling results reported in Supporting Table S1 were accurate to within 10% for even the coarsest simulated resolution of 4×4 mm^2.

The effect of bipolar gradients on flowing spins is demonstrated in-vivo in the coronal ^{1}H images of the kidney (Fig. 4). In the absence of bipolar gradients (Fig. 4A), signal from the vasculature (specifically the abdominal aorta and vena cava) appeared bright. After applying bipolar gradients (Fig. 4B), these vessels as well as the branching renal and segmental arteries were adequately suppressed. Higher b-values were found to have a minimal effect on the vasculature while further attenuating static signals undesirably. These results indicate that b = 32 s/mm^2 was empirically sufficient to null signal from fast flowing spins in the descending aorta in addition to slower spins in the vena cava, renal and segmental arteries.

Extending the simulation results to in-vivo ^{13}C imaging of renal metabolism also showed a substantial decrease in vascular signal (Fig. 5) confirming the general predictions from theory and simulation. SNR measurements of peak lactate in the kidney were similar for both experiments (SNR = 42 and 40, respectively), indicating that the diffusion gradient had a minimal effect on static spins. However, metabolite data fit to the two-site exchange model showed substantially different apparent rate constants, with whole kidney values of k_p = 0.020 s^{-1} and 0.012 s^{-1} with and without diffusion gradients, respectively. We attribute this difference to the reduced partial-volume contamination from vascular pyruvate.

DISCUSSION

In this paper, we have designed and implemented flow-sensitive gradients to mitigate partial-volume artifacts from the large vessels supplying the kidneys. In both simulations and experiments, signal from flowing spins was substantially suppressed as predicted, with negligible impact on static and slow flowing spins. Partial-volume effects from the vascular pyruvate signal were reduced with increased spatial resolution but with a deleterious decrease in SNR. Applying bipolar gradients reduced partial-volume artifacts that bias kinetic modeling without an appreciable decrease in SNR or an increase in scan time.

Alternative methods to better isolate intracellular metabolism are limited. A gadolinium (Gd) based solution could be administered after injection of hyperpolarized substrate to minimize the contribution of metabolites that reside in the vascular and extravascular/extracellular compartments (14). The use of flow dephasing gradients vs. paramagnetic agents is advantageous because in-flowing HP substrate signal is preserved for subsequent experiments rather than being completely or substantially depolarized. Moreover, clinically available Gd compounds have comparatively low longitudinal relaxivities (35) and outer sphere effects, which are the predominant relaxation mechanism for available Gd compounds interacting with ^{13}C carboxylic acids (36), scale inversely to distance of closest approach (37) and will therefore lead to increased relaxation of intracellular metabolites.

As an alternative to adding bipolar gradients, simulations show that partial volume effects from the murine renal vasculature could potentially be mitigated simply by increasing in-plane resolution to 1×1 mm^2. However, this comes at the cost of reduced SNR, which may be impractical for many applications due to finite magnetization. Moreover, improved spatial resolution would only reduce in-plane partial-volume effects, leaving through-plane partial-volume artifacts unaffected. These might include, for example, the renal and segmental arteries that branch off the abdominal aorta.

Bipolar gradients also result in signal reduction due to extended echo times and diffusion sensitization. This effect is expected to be negligibly small for our empirically determined optimal b-value of 32 s/mm^2, with a corresponding TE increase of 6.2 ms. Typical b-values used for diffusion-weighted imaging are on the order of 1000 s/mm^2 (38), or more than 30 times greater than those used in these experiments. Assuming unrestricted diffusion of ^{13}C metabolites, the signal loss in the extravascular/extracellular compartments for our b-value is expected to be only 5% (based on diffusion coefficients from (30)). Restricted diffusion, which occurs for intracellular metabolites, would lead to even lower signal attenuation. Removing the extravascular/extracellular metabolite signal would further increase the accuracy of kinetic modeling. However, the b-values required to completely isolate the intracellular space (39) are likely to be too high to be of use in imaging techniques.

It should be noted that there are several important limitations to the present study. Besides the small sample size, the amount of vascular suppression is directly related to variations in the intra-voxel velocity profile. The peak blood velocity and vessel size will be different for larger animals, potentially requiring a different b-value to adequately suppress flowing spins. Additionally, the flow velocity changes observed in-vivo lead to vascular suppression that is expected to be a function of the cardiac cycle (40). In principle, this can lead to varying amounts of phase accrual if cardiac triggering is not used, limiting the amount of vascular suppression that can be achieved. Investigating the degree and impact of this source of variation is outside the scope of the present feasibility study, but is an important area of future work. Furthermore, applying this technique to humans on a clinical scanner will pose technical challenges due to the reduced gradient performance on typical clinical systems. To achieve sufficient intra-voxel phase dispersion, the bipolar pulse width will have to increase to compensate for the lower gradient amplitude. Since the first gradient moment scales as δ^2, a comparable phase dispersion should be achievable with a factor of 2–3 increase in δ at equivalent blood velocities. The tradeoff would be a moderate increase in TE which should be tolerable given the relatively long T_2^* of ^{13}C-pyruvate in vivo. Empirical measures of the peak blood velocity in the ascending aorta of humans are comparable to that of mice, on the order of 90 cm/s (41,42), suggesting the proposed technique is feasible in patients on clinical systems.

Moreover, complex data reconstruction using model-based techniques is sensitive to phase errors (43,44). Despite the low b-value used in these experiments, phase errors due to gradient-induced eddy currents are likely to be present due in large part to the higher gradient strength needed to offset the lower ^{13}C gyromagnetic ratio ($\gamma(^{13}C) \approx ¼\ \gamma(^{1}H)$). Reducing the slew-rate or adding a delay before the start of data acquisition would limit such errors. Finally, improvements in modeling accuracy can only be proved indirectly through simulation, and we necessarily infer these improvements translate to in-vivo results. Further investigations are needed to confirm improved accuracy of kinetic modeling in-vivo with controlled interventions known to affect metabolic rates.

CONCLUSION

In hyperpolarized ^{13}C experiments, accurate measures of metabolite dynamics are critical to assessing the disease state and health of the tissues of interest. However, accurate kinetic

modeling is corrupted by outside vascular signal that doesn't directly contribute to metabolism within the tissue. By applying a bipolar gradient following excitation, flowing spins can be suppressed, removing contaminating signal from the vasculature in simulations and in-vivo experiments. Improved accuracy was observed for kinetic rates of metabolite conversion from pyruvate to lactate in simulations without sacrificing SNR or temporal resolution, suggesting similar improvements in-vivo.

Supplementary Material

Refer to Web version on PubMed Central for supplementary material.

Acknowledgments

Funding: NIH 1P50AG033514, Department of Medical Physics, NIH/NCI T32 CA009206 Radiological Sciences Training Grant, a Pilot Award from the UW-Carbone Comprehensive Cancer Center, and support from GE Healthcare.

References

1. Ardenkjær-Larsen JH, Fridlund B, Gram A, Hansson G, Hansson L, Lerche MH, Servin R, Thaning M, Golman K. Increase in signal-to-noise ratio of > 10,000 times in liquid-state NMR. Proc Natl Acad Sci USA. 2003; 100(18):10158–10163. [PubMed: 12930897]
2. Darpolor MM, Yen Y-F, Chua M-S, Xing L, Clarke-Katzenberg RH, Shi W, Mayer D, Josan S, Hurd RE, Pfefferbaum A, Senadheera L, So S, Hofmann LV, Glazer GM, Spielman DM. In vivo MRSI of hyperpolarized [1-13C]pyruvate metabolism in rat hepatocellular carcinoma. NMR Biomed. 2010:506–513. [PubMed: 21674652]
3. Harris T, Eliyahu G, Frydman L, Degani H. Kinetics of hyperpolarized 13C1-pyruvate transport and metabolism in living human breast cancer cells. Proceedings of the National Academy of Sciences. 2009; 106(43):18131–18136.
4. Kurhanewicz J, Vigneron DB, Brindle K, Chekmenev EY, Comment A, Cunningham CH, DeBerardinis RJ, Green GG, Leach MO, Rajan SS, Rizi RR, Ross BD, Warren WS, Malloy CR. Analysis of Cancer Metabolism by Imaging Hyperpolarized Nuclei: Prospects for Translation to Clinical Research. Neoplasia. 2011; 13(2):81–97. [PubMed: 21403835]
5. Albers MJ, Bok R, Chen AP, Cunningham CH, Zierhut ML, Zhang VY, Kohler SJ, Tropp J, Hurd RE, Yen Y-F, Nelson SJ, Vigneron DB, Kurhanewicz J. Hyperpolarized 13C Lactate, Pyruvate, and Alanine: Noninvasive Biomarkers for Prostate Cancer Detection and Grading. Cancer Res. 2008; 68(20):8607–8615. [PubMed: 18922937]
6. Day SE, Kettunen MI, Gallagher FA, Hu DE, Lerche M, Wolber J, Golman K, Ardenkjaer-Larsen JH, Brindle KM. Detecting tumor response to treatment using hyperpolarized 13C magnetic resonance imaging and spectroscopy. Nat Med. 2007; 13(11):1382–1387. [PubMed: 17965722]
7. Day SE, Kettunen MI, Cherukuri MK, Mitchell JB, Lizak MJ, Morris HD, Matsumoto S, Koretsky AP, Brindle KM. Detecting response of rat C6 glioma tumors to radiotherapy using hyperpolarized [1–13C]pyruvate and 13C magnetic resonance spectroscopic imaging. Magnetic Resonance in Medicine. 2011; 65(2):557–563. [PubMed: 21264939]
8. Josan S, Xu T, Yen Y-F, Hurd R, Ferreira J, Chen C-H, Mochly-Rosen D, Pfefferbaum A, Mayer D, Spielman D. In vivo measurement of aldehyde dehydrogenase-2 activity in rat liver ethanol model using dynamic MRSI of hyperpolarized [1-13C]pyruvate. NMR in Biomedicine. 2013; 26(6):607–612. [PubMed: 23225495]
9. Xu T, Mayer D, Gu M, Yen Y-F, Josan S, Tropp J, Pfefferbaum A, Hurd R, Spielman D. Quantification of in vivo metabolic kinetics of hyperpolarized pyruvate in rat kidneys using dynamic 13C MRSI. NMR in Biomedicine. 2011; 24(8):997–1005. [PubMed: 21538639]
10. Schroeder MA, Lau AZ, Chen AP, Gu Y, Nagendran J, Barry J, Hu X, Dyck JRB, Tyler DJ, Clarke K, Connelly KA, Wright GA, Cunningham CH. Hyperpolarized 13C magnetic resonance

reveals early- and late-onset changes to in vivo pyruvate metabolism in the failing heart. European Journal of Heart Failure. 2013; 15(2):130–140. [PubMed: 23258802]

11. Cheng H-LM. T1 measurement of flowing blood and arterial input function determination for quantitative 3D T1-weighted DCE-MRI. Journal of Magnetic Resonance Imaging. 2007; 25(5): 1073–1078. [PubMed: 17410576]
12. Haacke, EM. Magnetic Resonance Imaging: Physical Principles and Sequence Design. J. Wiley & Sons; 1999.
13. Chen AP, Leung K, Lam W, Hurd RE, Vigneron DB, Cunningham CH. Design of spectral-spatial outer volume suppression RF pulses for tissue specific metabolic characterization with hyperpolarized 13C pyruvate. Journal of Magnetic Resonance. 2009; 200(2):344–348. [PubMed: 19616981]
14. Smith M, Peterson E, Gordon J, Niles D, Rowland I, Kurpad K, Fain S. In-vivo imaging and spectroscopy of dynamic metabolism using simultaneous 13C and 1H MRI. Biomedical Engineering, IEEE Transactions on. 2011; (99):45–49. PP.
15. Josan S, Yen Y-F, Hurd R, Pfefferbaum A, Spielman D, Mayer D. Application of double spin echo spiral chemical shift imaging to rapid metabolic mapping of hyperpolarized [1-13C]-pyruvate. Journal of Magnetic Resonance. 2011; 209(2):332–336. [PubMed: 21316280]
16. Larson PEZ, Kerr AB, Reed GD, Hurd RE, Kurhanewicz J, Pauly JM, Vigneron DB. Generating Super Stimulated-Echoes in MRI and Their Application to Hyperpolarized C-13 Diffusion Metabolic Imaging. Medical Imaging, IEEE Transactions on. 2012; 31(2):265–275.
17. Swisher CL, Larson PEZ, Kruttwig K, Kerr AB, Hu S, Bok RA, Goga A, Pauly JM, Nelson SJ, Kurhanewicz J, Vigneron DB. Quantitative measurement of cancer metabolism using stimulated echo hyperpolarized carbon-13 MRS. Magnetic Resonance in Medicine. 2014; 71(1):1–11. [PubMed: 23412881]
18. Pell GS, Lewis DP, Branch CA. Pulsed arterial spin labeling using TurboFLASH with suppression of intravascular signal. Magnetic Resonance in Medicine. 2003; 49(2):341–350. [PubMed: 12541255]
19. Ye FQ, Mattay VS, Jezzard P, Frank JA, Weinberger DR, McLaughlin AC. Correction for vascular artifacts in cerebral blood flow values measured by using arterial spin tagging techniques. Magnetic Resonance in Medicine. 1997; 37(2):226–235. [PubMed: 9001147]
20. Lin H-Y, Flask CA, Dale BM, Duerk JL. Rapid dark-blood carotid vessel-wall imaging with random bipolar gradients in a radial SSFP acquisition. Journal of Magnetic Resonance Imaging. 2007; 25(6):1299–1304. [PubMed: 17520723]
21. Hamilton CA, Moran PR, Peter Santago II, Rajala SA. Effects of intravoxel velocity distributions on the accuracy of the phase-mapping method in phase-contrast MR angiography. Journal of Magnetic Resonance Imaging. 1994; 4(5):752–755. [PubMed: 7981522]
22. Pipe JG. A simple measure of flow disorder and wall shear stress in phase contrast MRI. Magnetic Resonance in Medicine. 2003; 49(3):543–550. [PubMed: 12594758]
23. Dyverfeldt P, Sigfridsson A, Kvitting J-PE, Ebbers T. Quantification of intravoxel velocity standard deviation and turbulence intensity by generalizing phase-contrast MRI. Magnetic Resonance in Medicine. 2006; 56(4):850–858. [PubMed: 16958074]
24. Stejskal E, Tanner J. Spin diffusion measurements: spin echoes in the presence of a time-dependent field gradient. The Journal of chemical physics. 1965; 42(1):288.
25. Le Bihan D, Turner R. Intravoxel incoherent motion imaging using spin echoes. Magnetic Resonance in Medicine. 1991; 19(2):221–227. [PubMed: 1881307]
26. Bernstein, M.; King, K.; Zhou, X. Handbook of MRI Pulse Sequences. Academic Press; 2004.
27. Glover GH. Simple analytic spiral K-space algorithm. Magnetic Resonance in Medicine. 1999; 42(2):412–415. [PubMed: 10440968]
28. Reeder SB, Brittain JH, Grist TM, Yen Y-F. Least-squares chemical shift separation for 13C metabolic imaging. Journal of Magnetic Resonance Imaging. 2007; 26(4):1145–1152. [PubMed: 17896366]
29. Zhao X, Pratt R, Wansapura J. Quantification of aortic compliance in mice using radial phase contrast MRI. Journal of Magnetic Resonance Imaging. 2009; 30(2):286–291. [PubMed: 19629988]

30. Koelsch BL, Keshari KR, Peeters TH, Larson PEZ, Wilson DM, Kurhanewicz J. Diffusion MR of hyperpolarized 13C molecules in solution. Analyst. 2013; 138(4):1011–1014. [PubMed: 23304699]
31. Zhao L, Mulkern R, Tseng C-H, Williamson D, Patz S, Kraft R, Walsworth RL, Jolesz FA, Albert MS. Gradient-Echo Imaging Considerations for Hyperpolarized129Xe MR. Journal of Magnetic Resonance, Series B. 1996; 113(2):179–183.
32. Gordon, JW.; Fain, SB.; Johnson, KM. Direct Estimation of Hyperpolarized Metabolites with IDEAL Spiral CSI; Proceedings of the 20th Annual Meeting of ISMRM; Melbourne, Australia. 2012. Abstract 4299
33. Wiesinger F, Weidl E, Menzel MI, Janich MA, Khegai O, Glaser SJ, Haase A, Schwaiger M, Schulte RF. IDEAL spiral CSI for dynamic metabolic MR imaging of hyperpolarized [1–13C]pyruvate. Magnetic Resonance in Medicine. 2012; 68(1):8–16. [PubMed: 22127962]
34. Duyn JH, Yang Y, Frank JA, van der Veen JW. Simple Correction Method for k-Space Trajectory Deviations in MRI. Journal of Magnetic Resonance. 1998; 132(1):150–153. [PubMed: 9615415]
35. Gabellieri C, Leach MO, Eykyn TR. Modulating the relaxivity of hyperpolarized substrates with gadolinium contrast agents. Contrast Media Mol Imaging. 2009; 4(3):143–147. [PubMed: 19330792]
36. van Heeswijk RB, Laus S, Morgenthaler FD, Gruetter R. Relaxivity of Gd-based contrast agents on X nuclei with long intrinsic relaxation times in aqueous solutions. Magnetic Resonance Imaging. 2007; 25(6):821–825. [PubMed: 17448617]
37. Helm L. Relaxivity in paramagnetic systems: Theory and mechanisms. Prog Nucl Magn Reson Spectrosc. 2006; 49(1):45–64.
38. Alexander AL, Lee JE, Lazar M, Field AS. Diffusion Tensor Imaging of the Brain. Neurotherapeutics. 2007; 4(3):316–329. [PubMed: 17599699]
39. Koelsch, BL.; Keshari, KR.; Peeters, TH.; Larson, PEZ.; M, WD.; Kurhanewicz, J. Complete Separation of Extra- And Intracellular Hyperpolarized 13C Metabolite Signal with Diffusion Weighted MR; Proceedings of the 21st Annual Meeting of ISMRM; Salt Lake City, USA. 2013. Abstract 567
40. Srichai MB, Lim RP, Wong S, Lee VS. Cardiovascular Applications of Phase-Contrast MRI. American Journal of Roentgenology. 2009; 192(3):662–675. [PubMed: 19234262]
41. Hartley CJ, Michael LH, Entman ML. Noninvasive measurement of ascending aortic blood velocity in mice. American Journal of Physiology – Heart and Circulatory Physiology. 1995; 268(1):H499–H505.
42. Gardin JM, Burn CS, Childs WJ, Henry WL. Evaluation of blood flow velocity in the ascending aorta and main pulmonary artery of normal subjects by Doppler echocardiography. American Heart Journal. 1984; 107(2):310–319. [PubMed: 6695664]
43. Hernando D, Hines CDG, Yu H, Reeder SB. Addressing phase errors in fat-water imaging using a mixed magnitude/complex fitting method. Magnetic Resonance in Medicine. 2012; 67(3):638–644. [PubMed: 21713978]
44. Yu H, Shimakawa A, Hines CDG, McKenzie CA, Hamilton G, Sirlin CB, Brittain JH, Reeder SB. Combination of complex-based and magnitude-based multiecho water-fat separation for accurate quantification of fat-fraction. Magnetic Resonance in Medicine. 2011; 66(1):199–206. [PubMed: 21695724]

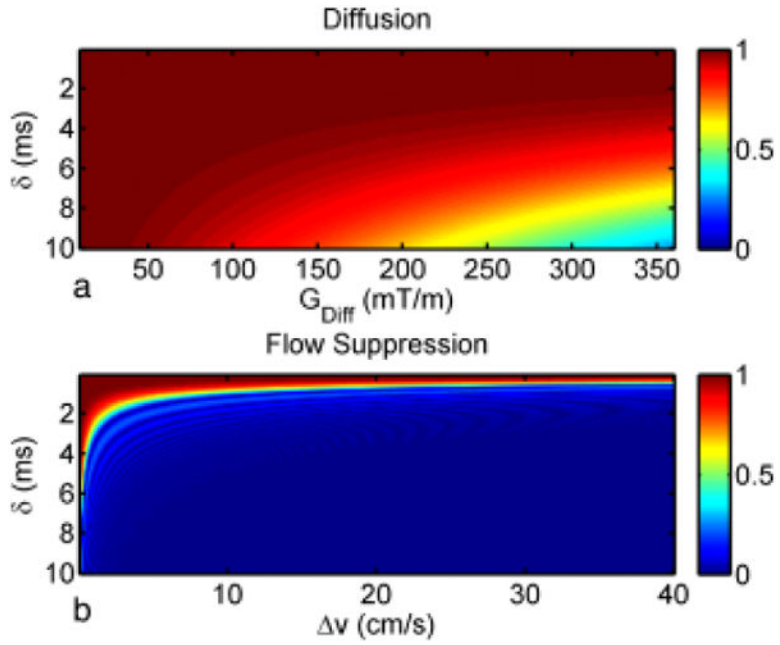

Figure 1.

Analytical plots of the relationship between phase dispersion and diffusion weighting are presented. Normalized signal due to diffusion weighting (A) is displayed as a function of bipolar gradient pulse width and amplitude for Eq. 5. Flow suppression calculations (B) are plotted as a function of bipolar gradient pulse width and peak blood velocity for Eq. 3. Together, these plots indicate a large parameter space that can suppress a range of velocities expected in the macro-vasculature without significant signal loss due to metabolite diffusion. Flow suppression calculations assumed a fixed gradient strength of 360 mT/m to minimize the TE and signal loss from T_2^* relaxation

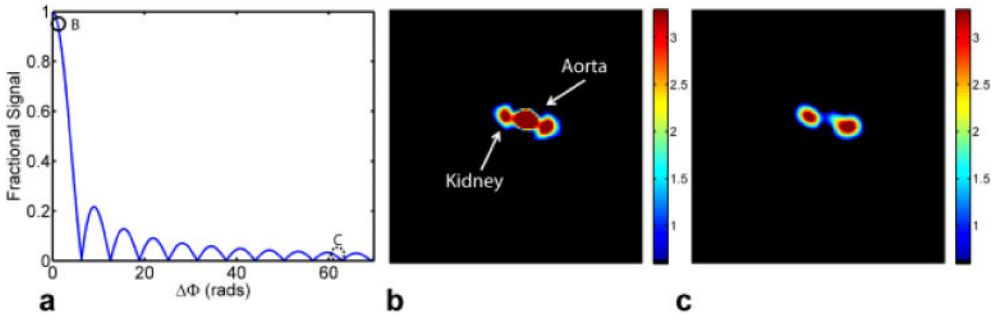

Figure 2.

Simulated intravoxel signal loss in the presence of laminar flow (Eq. 3b) without (B, solid open circle in 2A) and with (C, dashed open circle in 2A) bipolar gradients using the values selected from the analytical parameter space in Fig. 1 (G_{diff} = 360 mT/m and T = 3.1 ms). In the absence of bipolar gradients, signal from the central vasculature leads to partial-volume effects that interfere with nearby organ voxels (B). When bipolar gradients are applied, the spatially varying velocity profile leads to signal loss from intravoxel phase dispersion (C).

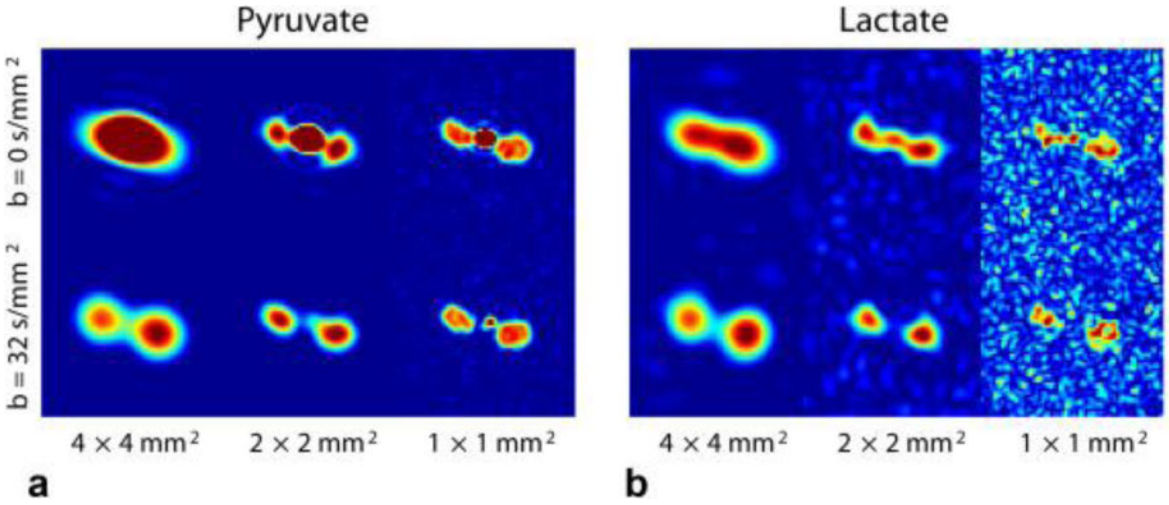

Figure 3.

Simulations showing the effect of spatial resolution for (A) [1-^{13}C]pyruvate and (B) [1-^{13}C]lactate images. Images are from peak SNR timeframes acquired without (top row) and with (bottom row) bipolar gradients using a spiral trajectory. In-plane resolution increases along columns in both panels A and B from left to right from 4×4 mm^2, 2×2 mm^2 and 1×1 mm^2, respectively. Partial-volume effects from the vascular pyruvate signal were reduced with increased spatial resolution but with an expected decrease in SNR. With bipolar gradients, the vascular signal was effectively suppressed at all simulated resolutions with negligible additional SNR loss. The metabolite maps have been normalized to the same signal intensity to illustrate the reduced SNR at finer spatial resolutions.

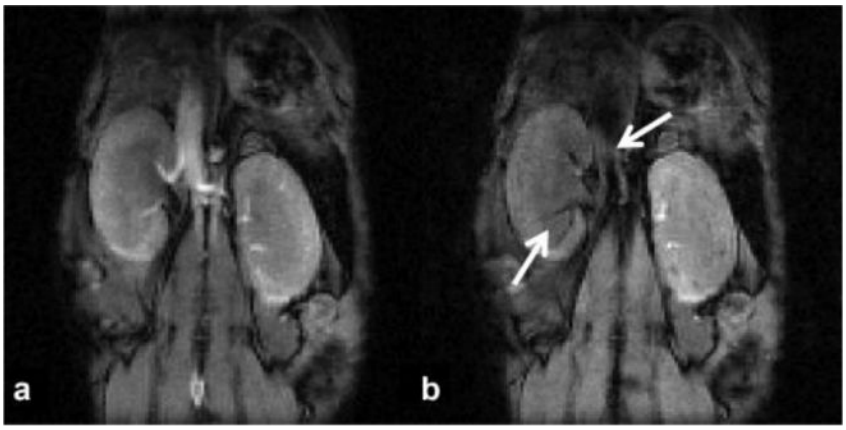

Figure 4.

In-vivo experiment showing coronal ^{1}H images in the absence (A) and presence (B) of bipolar diffusion gradients with a b-value of 32 s/mm^2. Note the signal loss from the aorta, vena cava, renal and segmental arteries (white arrows in B) observed with the application of the bipolar pulse.

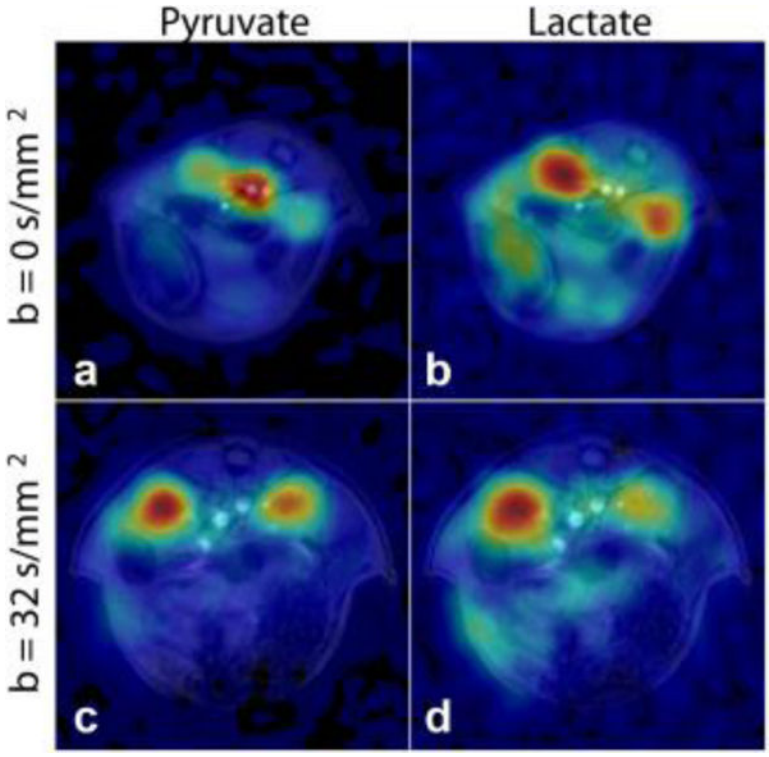

Figure 5.

In-vivo experiment showing the effect of bipolar gradients on renal metabolism. The strong vascular pyruvate signal from the aorta (A) led to partial-volume effects with kidney voxels, confounding accurate measures of metabolism. The application of a bipolar gradient reduced the vascular signal (C), increasing kidney conspicuity and mitigating partial-volume effects. Lactate images (B, D) remained relatively unaffected (SNR = 42 and 40, respectively), while kinetic rates were substantially changed.